Supramolecular Bionanocomposites, Part 2: Effects of Carbon Nanoparticle Surface Functionality on Polylactide Crystallization

Margaret J. Sobkowicz, Rodolfo Sosa, John R. Dorgan

Department of Chemical and Biochemical Engineering, Colorado School of Mines, Golden, Colorado 80401

Received 29 June 2010; accepted 22 November 2010
DOI 10.1002/app.33787
Published online 14 March 2011 in Wiley Online Library (wileyonlinelibrary.com).

ABSTRACT: Two types of supramolecular carbon nanostructures, carbon nanospheres (CNS) and multiwalled carbon nanotubes, (MWCNTs) are investigated for their potential as nanofillers in the bioplastic polylactide (PLA). Modification of the surfaces of both carbon nanostructures by covalent attachment of dodecylamine is accomplished and the effects of this compatibilizing functionality are explored. Crystallization kinetics, thermal properties, and mechanical properties are investigated. Addition of a small amount of carbon to the PLA increases the thermal stability by as much as 20–30°C. Incorporation of the MWCNT and CNS increases the heat distortion temperature by up to 10°C. Speed up in crystallization rate is observed for small to intermediate loading levels; however, at higher nanofiller loading, the rate decreases. Functionalized nanostructures are more effective at increasing crystallization rates than unfunctionalized nanostructures. It is concluded that the dodecylamine (DDA) grafted to the carbon surfaces aids in dispersing the materials and preventing aggregation, thereby providing higher surface area for heterogeneous nucleation of the biopolymer. The resulting materials are composed of the supramolecular carbon nanostructure embedded in a semicrystalline biopolymer matrix. © 2011 Wiley Periodicals, Inc. J Appl Polym Sci 121: 2029–2038, 2011

Key words: nanocomposites; bioplastic(s); polylactide; poly(lactic acid); carbon nanostructures; renewable resources; sustainability

INTRODUCTION

Carbon fillers have been used as reinforcement in polymer composites since synthetic plastics were first developed. Carbon black is commonly incorporated in automotive tires to increase toughening and wear resistance. More recently, carbon nanotubes (CNTs) and fullerenes have been investigated for their potential to provide strength, toughening,[1] and unique electrical, optical,[2] and thermal[3] properties to all sorts of polymer matrices.[4,5] Nanomedicines or nanoparticles with tethered drug molecules and cell-specific target molecules are also of expanding interest. Potential applications for CNT-polymer nanocomposites include targeted drug delivery,[6] photovoltaics,[7] electromagnetic shielding materials,[8] and reinforced fibers and thermoplastics for aeronautical, automotive, sporting, and other high-performance applications.[9]

One of the biggest challenges in successful nanocomposite preparation is dispersion and distribution of nanoparticles in the polymer.[10] Nanoparticles tend to aggregate due to their high surface energy, and unfunctionalized CNTs are not generally soluble in any organic solvent.[11] Techniques explored to encourage dispersion include (1) extensive mechanical work in the form of shear or ultrasonication, (2) compatibilization using surfactants[12,13] or polymer wrapping,[14] and (3) covalent modification with small molecules or grafted polymer chains. Each technique has advantages and drawbacks and several thorough reviews are available on this important subject.[15,16] Successful dispersion of nanoparticles in polymers results in less aggregation of the filler, providing more surface area for interaction and improved mechanical and electrical properties at extremely low loading levels because of the efficient transfer of stress or charge through a percolated CNT network. Dynamic mechanical thermal analysis (DMTA) shows an increase in composite stiffness and glass transition temperatures.[17–19] Surface functionalization can also lead to a more pronounced effect on mechanical and other properties.[20]

Correspondence to: J. R. Dorgan (jdorgan@mines.edu).

Contract grant sponsor: National Research Initiative Competitive Grant from the USDA Cooperative State Research, Education, and Extension Service; contract grant number: 2006-35504-16618.

Contract grant sponsor: National Science Foundation; contract grant number: CMMI-0700869.

Contract grant sponsor: Colorado Center for Biorefining and Biofuels.

Polylactide (PLA) is an emerging green bioplastic; it is a semicrystalline polyester produced commercially from renewable resources. Applications for PLA are limited by its brittleness and low heat distortion temperature[21] making it a great candidate for property improvement through nanocomposite technology. PLA is of interest for compostable packaging[22] and fibers, and also in medical fields because of its biodegradability and biocompatibility.[21] PLA based bionanocomposites are of interest for biological sensing and drug delivery applications as well as production of high-performance biodegradable plastics. Carbon nanospheres (CNS) produced from cellulose[23] are a novel, synergistic nanofiller for PLA because the resulting composites are over 99% renewable. Because CNTs can be produced from renewable resources,[24] supramolecular bionanocomposites composed of PLA chains grafted to CNS or nanotubes[25,26] are also very high in renewable content. In the first of this series of articles, PLA was successfully grafted to both CNS and CNTs;[27] in this and the following report, related supramolecular surface modified CNSs and CNTs are embedded in PLA matrices to form novel bionanocomposites.

Biodegradation of PLA is strongly affected by crystallinity and crystalline form,[28,29] and as with most semicrystalline polymers, the degree of crystallinity and thermal history have a large influence on PLA's resulting thermomechanical properties.[27] Commercially-produced PLA is composed mostly of L-lactic acid with small amounts of D-lactic acid and is, therefore, notably slow to crystallize,[30] leading to prohibitively expensive processing. In a previous work, CNS were investigated as nucleating agents in PLA and polypropylene.[31] Carbon black and CNTs have also been shown to improve crystallization kinetics in PLA,[32,33] polypropylene,[34–37] and other polymer matrices.[38,39] Other materials investigated as nucleating agents for PLA include nanoclay,[40] talc,[41] and PLLA/PDLA stereocomplex crystallites.[42,43] Despite these successes, there remains a need to increase the crystallization rate of PLA and to explore synergistic effects of various fillers on nanocomposite properties.

In this work, two types of supramolecular carbon nanostructures, novel cellulose-derived CNS and multiwalled CNTs (MWCNTs), are investigated for their potential as nanofillers in PLA. Of particular interest are faster crystallization, increased heat distortion temperature, and improved thermal degradation of commercial-grade PLA. Modification of the surfaces of both carbon nanostructures with covalent attachment of dodecylamine (DDA) is accomplished and the effects of this compatibilizing functionality are explored with regard to crystallization kinetics and thermal and mechanical properties. Significant improvements of 20–30°C in thermal stability, 10°C increase in heat distortion temperature, and three times faster crystallization are observed. The resulting supramolecular bionanocomposites are unique in that the polymer matrix can be degraded either by hydrolysis or via biodegradation.[44]

EXPERIMENTAL METHODS

Chloroform, methanol, DDA, *N*,*N*-dimethylformamide (DMF), and thionyl chloride were reagent grade and used as received. CNS were obtained from Fullerene Sciences (Boulder, CO). MWCNT functionalized with hydroxyl groups (MWCNT-OH) and unfunctionalized MWCNT were from CheapTubes.com. PLA 2000D grade (extrusion/thermoforming, MFI 4–8 g/10 min) was obtained from NatureWorks LLC and dried by crystallization at 80°C under vacuum for at least 14 h before use.

CNS and MWCNT-OH were refluxed in thionyl chloride (3.33 mg/mL) with a small amount of DMF (1 mL per 30 mL thionyl chloride). After filtering (CNS, 0.1 μm nylon filter) or centrifuging (MWNCT, 10 min at 8600 g) and washing with chloroform, the acyl chloride functionalized CNS or MWCNT were added to melted DDA at a 10-fold stoichiometric excess relative to atomic carbon. The CNS or MWCNT were stirred in DDA 24 h, then diluted with chloroform and filtered (CNS) or centrifuged (MWCNT) to remove unreacted DDA. The resulting CNS-DDA or MWCNT-DDA was washed repeatedly until thermaogravimetric analysis (TGA) measurements indicated a stable amount of grafted functionality. Additional details are available in the literature.[45]

A solution blending technique was used to prepare the nanocomposites. A 10-wt % solution of PLA in chloroform was stirred overnight to ensure complete dissolution. Chloroform was also used to prepare 1 wt % suspensions (~ 15 mg/mL) of CNS, MWCNT, MWCNT-OH, CNS-DDA, and MWCNT-DDA thoroughly dried carbon samples. The carbon suspensions were then sonicated for 24 h and added in appropriate ratios to the PLA solution to target nominal compositions of 0.5, 2, 4, 7, and 12 wt % (CNS and MWCNT-OH) and 0.5, 2, 7, and 12 wt % (CNS-DDA and MWCNT-DDA). Solution-phase composites were stirred on magnetic stir plates for 48 h and then precipitated into 10-fold excess methanol. Precipitate was collected, dried overnight, and further dried under vacuum (25 inHg) at 60°C for at least 24 h. Hereafter, nanocomposite samples will be indicated using the nominal weight fraction followed by the type of carbon nanostructure and the functionality, if present (for example 0.5CNS-PLA, 12MWCNT-DDA-PLA, etc).

TGA, to determine actual carbon weight loading and thermal stability, was run on a Seiko TG/DTA

220 calibrated against an indium standard. The sweep gas was air and it was assumed, based on measurements of pure PLA and pure carbon specimens, that all mass remaining at 400°C was graphitic carbon. Sample starting mass was 15–30 mg. The heating program was as follows: (1) heat from 30 to 800°C at 10°C/min, (2) hold 30 min at 800°C, and (3) cool from 800 to 30°C at 20°C/min.

Differential scanning calorimetry (DSC) was carried out on a Perkin Elmer DSC 7 calibrated against an indium standard. The instrument was cooled using ice water and nitrogen was used as the purge gas. The temperature program was as follows: (1) heat from 5 to 200°C at 10°C/min (2) hold at 200°C for 5 min (to erase thermal history), (3) cool to 110°C at 50°C/min, (4) hold 30 min at 110°C (isothermal crystallization), (5) cool to 5°C at 10°C/min, and (6) heat from 5 to 200°C at 10°C/min (record glass and melting transitions after crystallization). Two samples between 8 and 18 mg were run for each composite and resulting data were averaged.

Polarized optical microscopy was used to measure the spherulite growth rate for various composites. A small amount of lowest loading levels from each carbon composite was melted onto a glass slide and spread under the coverslip to a thickness of <1 mm. Each sample was heated in a Mettler Toledo FP82 hot stage and FP90 temperature controller (accuracy of ±0.2°C) to 180°C and held until completely melted for ~ 5 min. The melt was then quenched to 130°C and images were captured every minute for at least 30 min. Spherulite growth was measured and recorded for the lowest nanotube loading level of each composite type. ImageJ software was used to analyze the crystallization micrographs and the growth rates were taken to be the slopes of size vs. time plots.

DMTA was performed on a Rheometrics ARES-LS rheometer with torsional rectangular fixtures. Composite samples were vacuum/compression molded into rectangular bars ($3 \times 12.5 \times 45$ mm^3), crystallized at 110°C for 3 h (except for the uncrystallized sample of Fig. 1) and physically aged for 24 h before DMTA. Testing was carried out at 0.05% strain, 1 Hz, with a temperature ramp from 30 to 160°C at 5°C/min.

RESULTS AND DISCUSSION

The important influence of crystallinity on polymer properties is made clear by the data presented in Figure 1. Here, the shear moduli as a function of temperature during a DMTA heating scan for two PLA samples are presented. For the annealed and highly (about 40%) crystalline sample, the modulus drops by a single order of magnitude as the glass transition temperature (about 58°C) is passed. In comparison, the modulus of the amorphous sample drops precipitously by three orders of magnitude. With increasing temperature, the amorphous sample begins to crystallize at ~ 95°C, causing the modulus to actually increase with temperature. Clearly, in cases where temperature stability is important, a high degree of crystallinity is desirable. For economic reasons, it is important that this level of crystallinity is achieved rapidly so that manufacturing cycle time is minimized.

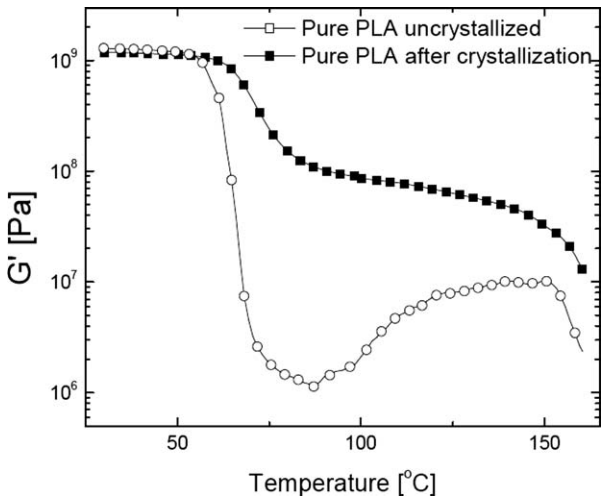

Figure 1 Storage modulus vs. temperature on heating for pure PLA before and after crystallization at 110°C.

The carbon nanostructures used in the present investigation have some novel features. Transmission electron microscopy (TEM) images of the two carbon nanoparticles are shown in Figure 2. The CNS are hollow with about 30 layers of graphene in the outer walls, and are 40 nm in diameter on average. The hydroxyl functionalized nanotubes (MWCNT-OH) are 20–30 nm in diameter and 10–30 μm in length, as reported by the manufacturer. These dimensions correspond to aspect ratios varying from 333 to 1500. The MWCNT-OH reportedly have 1.6 wt % OH functionality (0.011 mol fraction), surface area >110 m^2/g and electrical conductivity >100 S/cm. Before oxidation, the MWCNT-OH are identical to the unfunctionalized nanotubes (MWCNT). All three carbon nanostructures tend to aggregate in large bundles or tangles, when dried onto TEM grids.

Thermal stability

TGA scans for each composite are shown in Figures 3 and 4. The untreated CNS and MWCNT both have excellent thermal stability; neither loses significant mass until about 600°C. Hydroxylating the surface decreases thermal stability; the MWCNT-OH starts to lose mass at about 550°C. The data also show that CNS-DDA and MWCNT-DDA both lose the DDA

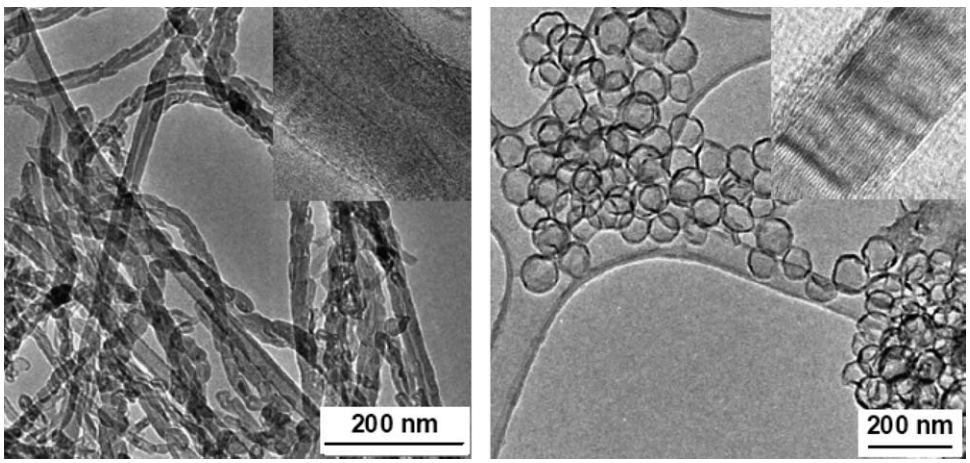

Figure 2 Representative TEM images of (left) MWCNT-OH and (right) CNS. Insets are close-up images of the nanostructure graphitic sidewalls.

functionality at relatively low temperatures. It appears that even addition of a small amount of carbon to the PLA increases the composites' overall thermal stability by as much as 20–30°C. However, there is not an appreciable increase in thermal stability after addition of more carbon. The TGA results allow the determination of actual, as opposed to nominal weight loadings. The percent carbon for each nanocomposite is taken as the remaining mass fraction at 425°C; at this temperature, both DDA and PLA are completely burned off.

Isothermal crystallization

Isothermal DSC crystallization curves are analyzed by taking the integral under the crystallization exotherm with respect to time and normalizing by division of the area under the entire peak. This procedure yields the fraction of achievable crystallinity as a function of time. Examples of two of the isothermal crystallization curves are shown in Figure 5(a); pure PLA is compared to a nanocomposite containing 7 wt % MWCNT-DDA. Because of the delay in sample temperature reaching T_c after the quench, there is an apparent onset time of a few seconds before integration starts. The integration end time was selected as the point at which the DSC curve returned to the baseline. Crystallization kinetics for the two cases are shown in Figure 5(b), which presents the corresponding crystalline fractions as a function of time.

Figure 6 shows the integration curves for all CNS-containing nanocomposites. In the left-hand plot, it is evident that unfunctionalized CNS do increase crystallization rates; however, there is no systematic trend with increasing CNS loading. In fact, the 15 wt % composite appears to crystallize as slowly as the pure PLA. In contrast, when the CNS-DDA are used, the crystallization rate increases considerably with each loading level. However, again at 13 wt %, the crystallization occurs more slowly than in the less loaded composites. A possible interpretation of these results is that the DDA functionalization improves dispersion, but that as the loading level

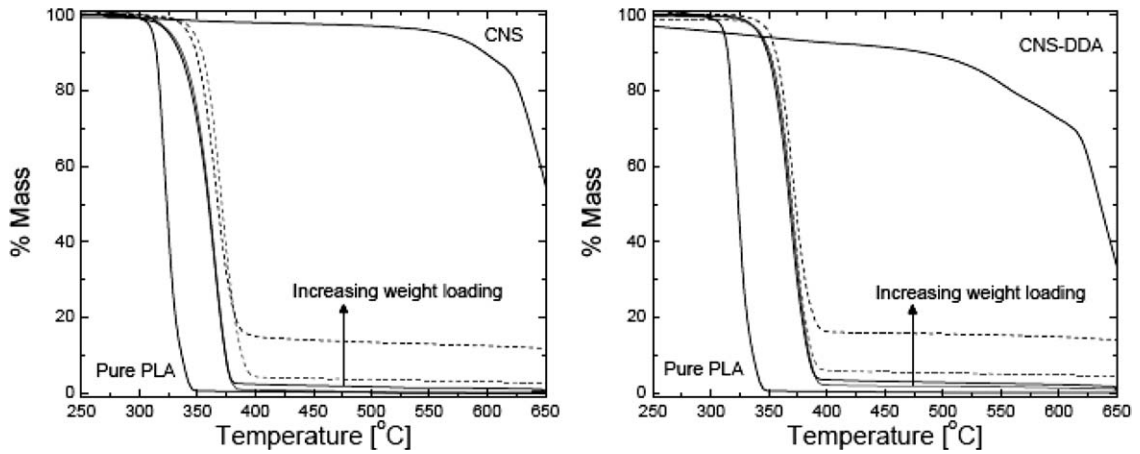

Figure 3 TGA thermal stability in air for (left) CNS composites and (right) CNS-DDA composites.

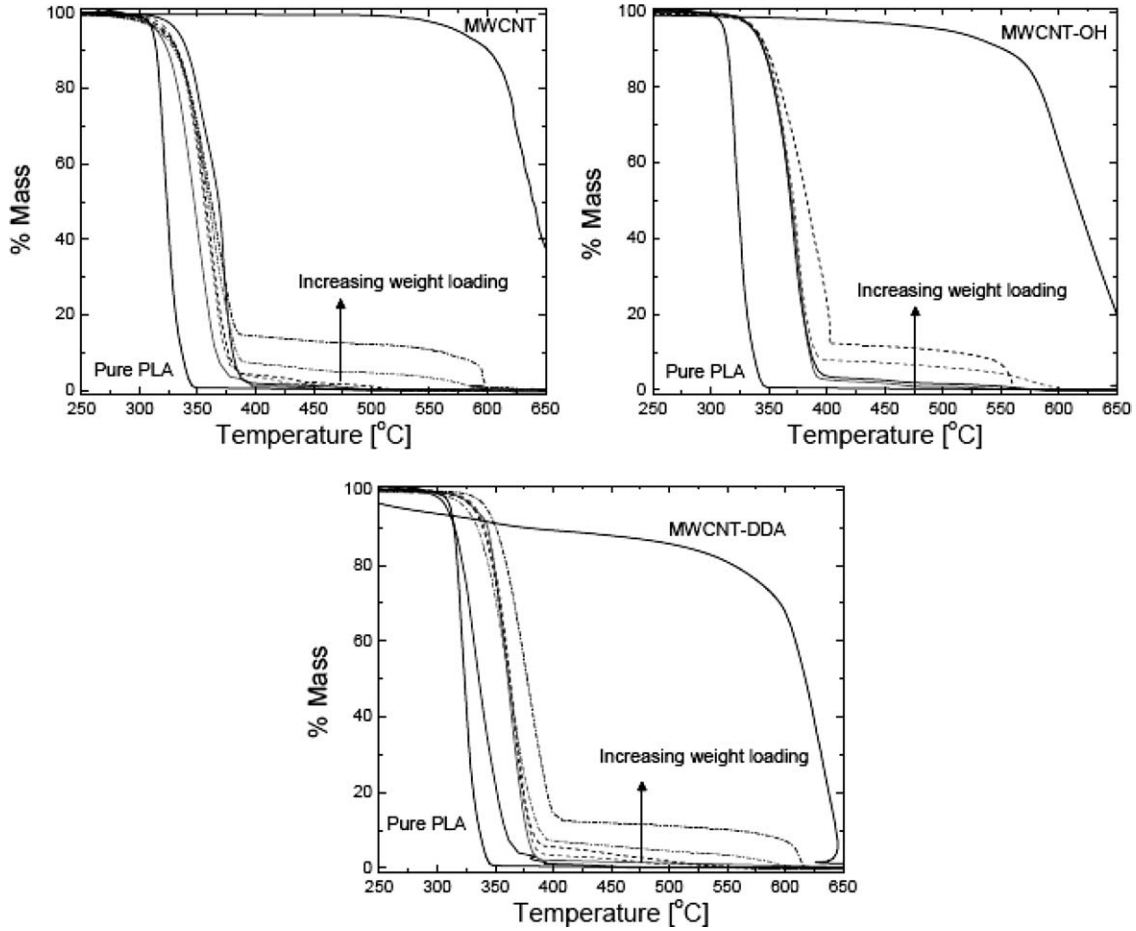

Figure 4 TGA thermal stability in air for (top left) MWCNT composites, (top right) MWCNT-OH composites, and (bottom) MWCNT-DDA composites.

increases a threshold is reached whereby concentration effects dominate and reaggregation of the nanofiller occurs.

Figure 7 shows similar results for MWCNT nanocomposites and for the control experiment of PLA blended with only DDA. In the case of MWCNT-OH, the smallest loading of CNTs appears to speed the crystallization somewhat, but addition of higher weight loadings does not increase the crystallization speed appreciably. For MWCNT, the lowest loading

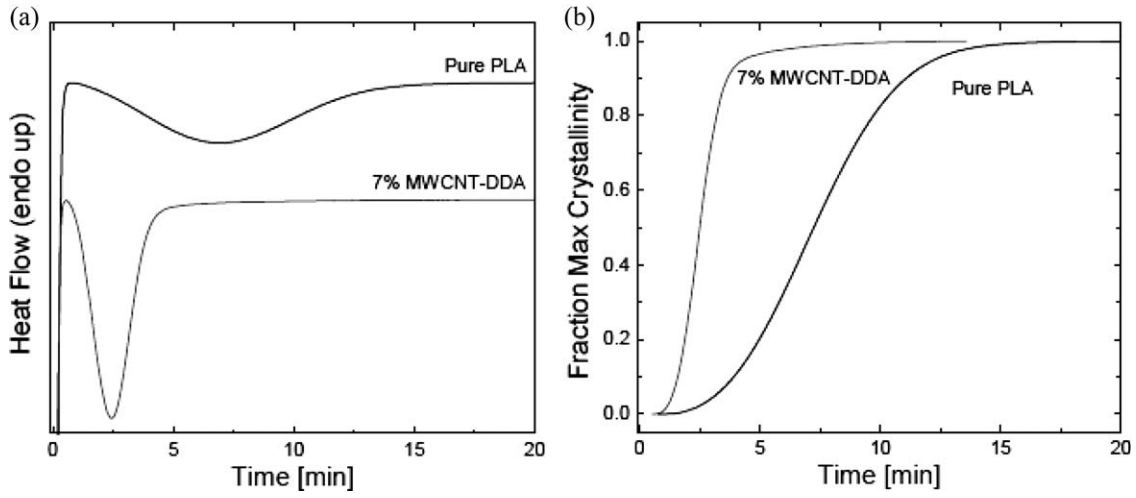

Figure 5 (a) Example DSC scans of isothermal crystallization exotherms for pure PLA and the fastest crystallizing composite, 7 wt % MWCNT-DDA. (b) Normalized, integrated curves for the same two samples.

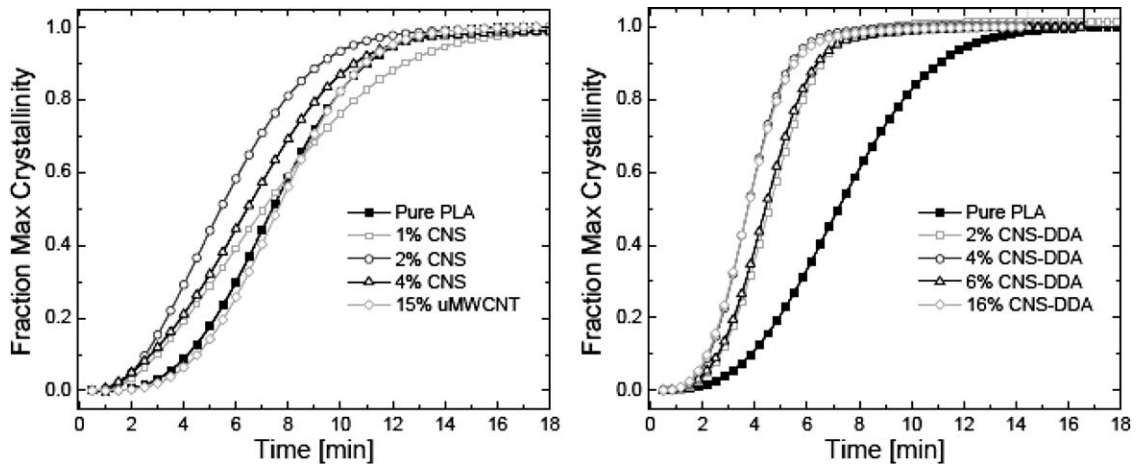

Figure 6 Integrated isothermal crystallization curves for (left) CNS-PLA composites and (right) CNS-DDA-PLA composites.

levels have no effect on the crystallization rate, whereas the higher levels show a slight increase in crystallization rate. In the case of MWCNT-DDA, the crystallization proceeds considerably faster up to addition of about 7 wt % MWCNT-DDA, but higher weight loadings are again less beneficial to accelerating crystallization kinetics.

The similarity of slower crystallization kinetics at very high loadings for both MWCNT-DDA and CNS-DDA indicates that either the nanoparticle

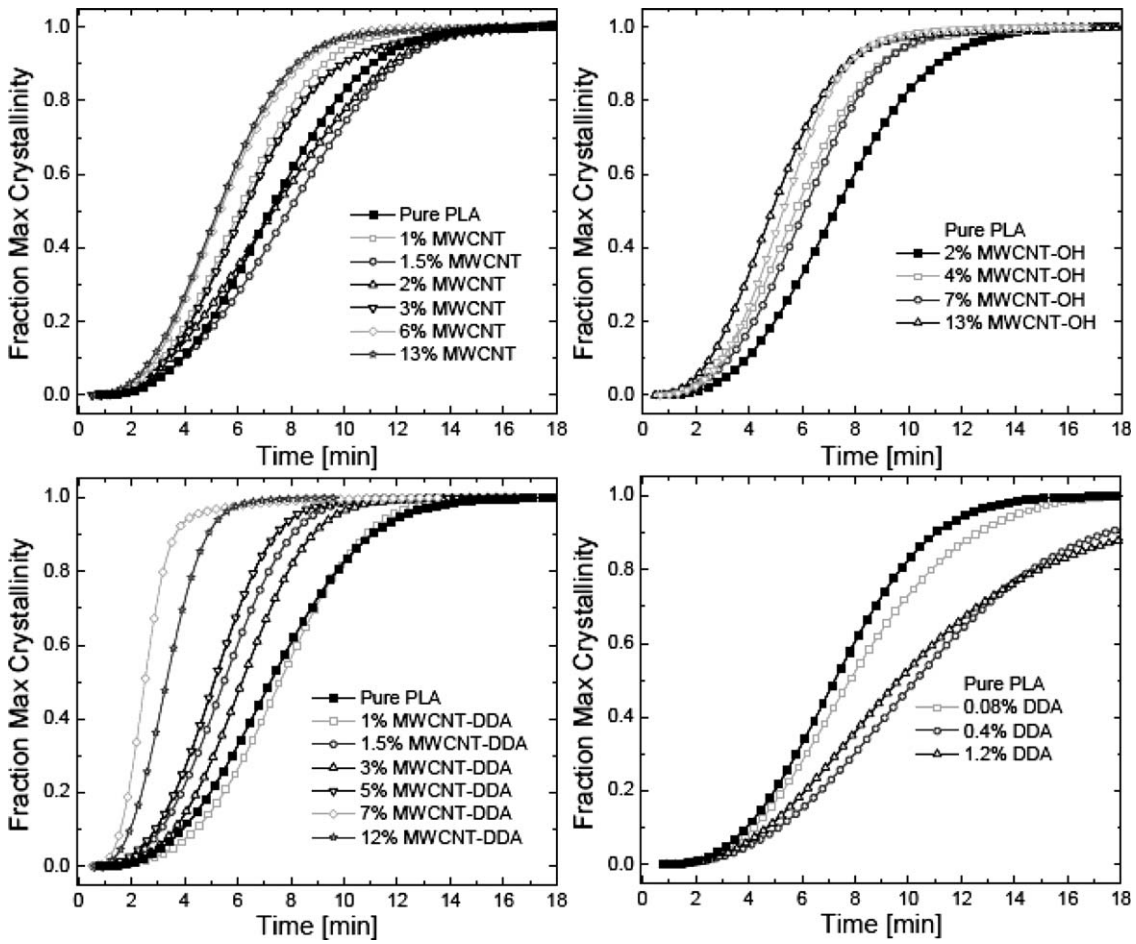

Figure 7 Integrated isothermal crystallization curves for (top left) MWCNT-PLA composites, (top right) MWCNT-OH-PLA composites, (bottom left) MWCNT-DDA-PLA composites, and (bottom right) DDA blended with PLA.

TABLE I
Summary of Thermal Data for All Composites Studied

Sample	Wt % (TGA)	$t_{1/2}$ (min) (± 0.01)[a]	ΔH_m (J/g)	%X (± 0.5)[a]	T_g (DSC) (°C) (± 1.0)[a]	HDT (DMTA) (°C)
PLA0	0.0	7.2	39.8	42.5	62.3	76.1
1MWCNT	1.1	6.0	38.0	41.0	62.3	76.6
1.5MWCNT	1.5	7.9	37.3	40.0	62.5	76.6
2MWCNT	1.9	7.3	36.8	40.0	62.9	77.2
3MWCNT	3.2	6.2	35.9	39.9	61.8	76.3
6MWCNT	6.4	5.3	34.0	39.1	62.7	78.1
13MWCNT	13.7	5.5	32.3	40.2	62.3	87.5
2MWCNT-OH	3.2	5.7	38.3	42.2	62.3	75.2
4MWCNT-OH	4.3	6.1	38.9	43.4	62.6	80.5
7MWCNT-OH	6.9	4.9	39.2	45.0	62.0	77.0
13MWCNT-OH	12.8	5.3	37.8	46.2	63.6	83.8
1MWCNT-DDA	0.9	7.6	37.4	40.1	62.9	77.3
1.5MWCNT-DDA	1.9	7.6	37.4	40.1	62.9	77.1
3MWCNT-DDA	2.9	5.5	37.0	40.7	62.5	77.5
5MWCNT-DDA	4.8	5.1	37.0	41.5	62.1	78.3
7MWCNT-DDA	7.2	2.6	37.8	43.5	63.0	78.3
12MWCNT-DDA	12.2	3.3	38.2	46.5	62.1	84.2
0.08DDA	0.1	12.6	40.1	42.8	60.6	75.2
0.4DDA	0.4	11.6	39.0	41.8	60.5	74.1
1.2DDA	1.2	12.0	41.6	44.9	60.3	73.7
1CNS	1.4	5.4	38.2	41.3		76.1
2CNS	2.4	5.4	39.3	43.0	63.7	77.5
4CNS	4.4	6.08	38.7	43.1	62.5	77.3
15CNS	15.1	7.98	32.1	39.5	63.4	81.3
2CNS-DDA	2.2	4.55	38.3	41.8	62.1	76.9
4CNS-DDA	3.6	4.6	40.1	44.4		79.6
6CNS-DDA	6.0	4.47	36.2	40.7	63.1	80.5
16CNS-DDA	16.4	3.96	34.1	40.7	62.0	81.3

[a] Error is calculated from the standard deviation of four samples from the same composite run separately through the crystallization DSC protocol.

clusters can impede crystal formation, or that a critical filler loading has been reached so that aggregation phenomena result in less surface area available for heterogeneous nucleation. Figure 6(d) shows the integration results from isothermal crystallization of PLA solution blended with pure DDA. It is clear that the presence of DDA alone actually slows crystallization down; therefore, it cannot be responsible for the faster crystallization in MWCNT-DDA and CNS-DDA composites. It can be concluded that the DDA grafted to the carbon surfaces aids in dispersing the materials and preventing aggregation, thereby providing higher surface area for nucleation of the polymer.

Table I lists the numerical results from TGA and DSC crystallization measurements. The actual weight loadings are listed as determined from TGA. For the best nucleator, 7MWCNT-DDA, 50% of max crystallinity ($t_{1/2}$) is reached nearly three times faster than pure PLA. Percent crystallinity values were calculated from the melting peak recorded after isothermal crystallization according to eq. (1),

$$\%X = \frac{\Delta H_m}{(1-w)\Delta H_m^{100}}, \quad (1)$$

where ΔH_m is the enthalpy of melting, or the area under the endotherm divided by sample mass, w is the mass fraction carbon in the sample, and ΔH_m^{100} is the theoretical enthalpy of melting for 100% crystalline PLA, taken as 93.7 J/g.[46] It is interesting to note that T_g values are close to those of pure PLA for all composites, indicating that no significant confinement of the polymer is occurring at the interface between the polymer and the nanoparticles. Percent crystallinity appears to decrease slightly in the case of unfunctionalized MWCNT, whereas it increases slightly for the OH- and DDA-functionalized MWCNT, but no clear trend is observed for the CNS. Crystallization mechanism and crystalline form are likely the same as those of the pure polymer.

Optical microscopy studies further reveal that the primary reason for enhanced crystallization kinetics must be denser nucleation. Within the experimental margin of error (±1.4 μm/min), the spherulite growth rates for the lowest weight fraction nanocomposites are the same as the growth rates in pure PLA. Figure 8 shows examples of the crystallization photos used for measurement of spherulite growth rate along with the spherulite growth rate for each composite. The lowest weight loaded samples are used to measure the growth rate because at the highest weight loadings the

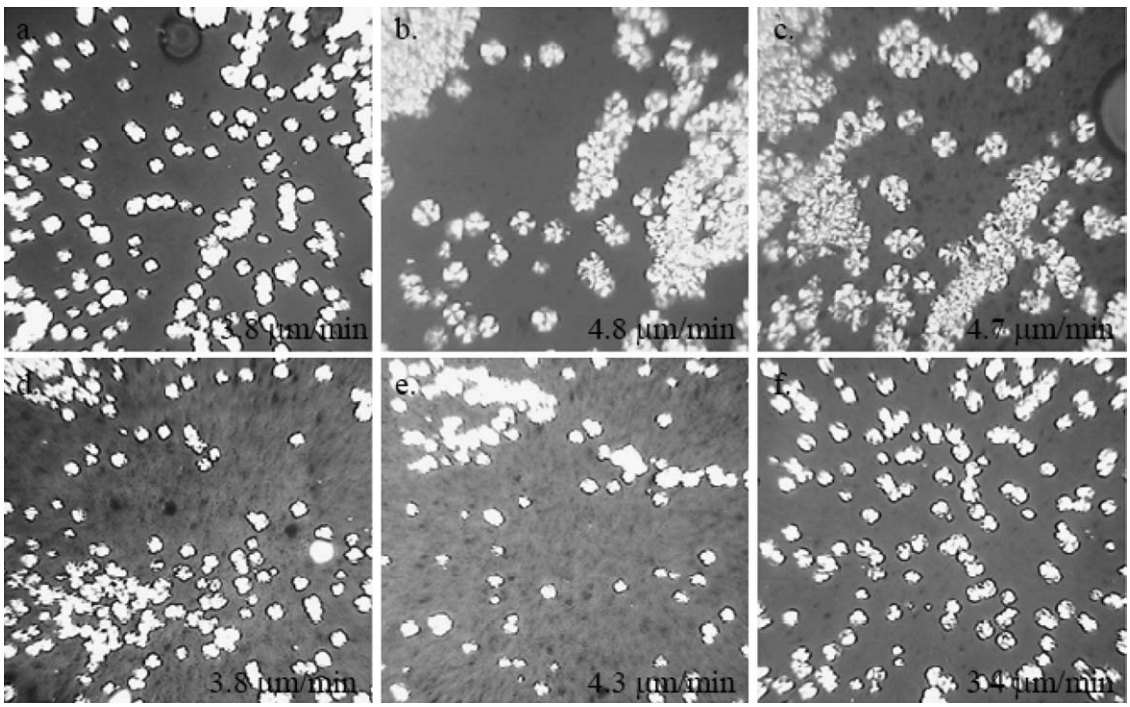

Figure 8 Optical micrographs (×10) after 15 min isothermal crystallization at 130°C; (a) 0.08DDA, (b) 1CNS, (c) 2CNS-DDA, (d) 1MWCNT, (e) 1MWCNT-OH, and (f) 1MWCNT-DDA solution blended with PLA. Growth rates in the lower right corners are the same within experimental error (standard deviation = 1.4 μm/min).

spherulites become obscured by the carbon inclusions in the samples and their size is difficult to measure. From the images of Figure 8, it appears that the carbon nanostructures are not completely dispersed down to individual nanoscale particles, and some larger scale aggregates are present, but the distribution appears even throughout the samples.

Dynamic mechanical thermal analysis

DMTA results for some of the nanocomposites are shown in Figure 9. Incorporation of either CNS or MWCNT raises the storage modulus in both the glassy (<60°C) and rubbery (>100°C) regions. The MWCNT have a slightly larger effect than the CNS at equivalent loading levels. The polymer chains can likely intercalate the web-like structure of the MWCNT to some degree, leading to a larger reinforcing effect. The effect is not as large as might be expected because of the high aspect ratio of the MWCNT, indicating that the tubes are not completely dispersed. The surface functionality of the CNS and the MWCNT seems to have little to no effect on the mechanical reinforcement. In fact, the

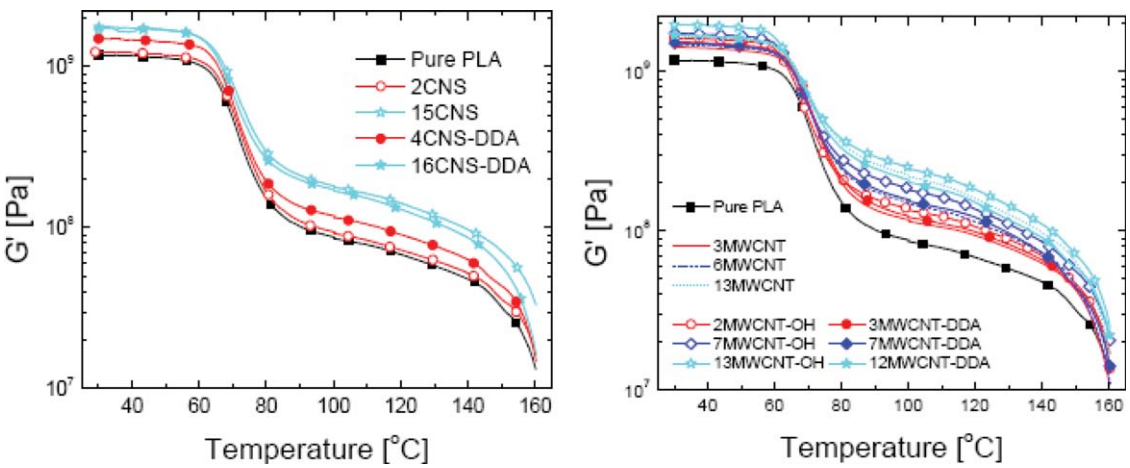

Figure 9 DMTA storage modulus for (left) CNS composites and (right) MWCNT composites. [Color figure can be viewed in the online issue, which is available at wileyonlinelibrary.com.]

MWCNT-OH composites have slightly larger moduli than the MWCNT and MWCNT-DDA composites at comparable loading levels. This may be due to hydrogen bonding interactions with the PLA matrix or between CNTs leading to a percolated network in which the tubes are resistant to slipping past one another. The composites' loss moduli showed similar increases indicating a stiffer and more solid-like material with increasing loading for all nanocomposites.

As mentioned in the Introduction section, PLA has a low heat distortion temperature, and this is an important limitation on the use of PLA. The HDT can be taken as the point at which the Young's modulus falls below 0.75 GPa.[47] Young's modulus is calculated from the storage modulus (G'), loss modulus (G''), and Poisson's ratio ($\nu = 0.333$ for PLA) using eq. (2):

$$E = 2(1+\upsilon)\left(G'^2 + G''^2\right)^{1/2} \quad (2)$$

Table I shows the HDT for all of the nanocomposites. Incorporation of the MWCNT and CNS increases the HDT by $\sim 10^\circ$C at a loading level of 13 wt % MWCNT.

CONCLUSIONS

In this study, two different carbon nanofiller geometries are investigated as crystal nucleators for PLA. The effects of a DDA grafted surface functionality on thermal, mechanical, and crystallization properties are explored. It is shown through TGA studies that the added carbon nanoparticles increase the thermal degradation temperature of the composites by 20–30°C over the neat polymer.

It is found that while pure DDA slows the polymer crystallization, DDA-grafted CNS and MWCNT increase the crystallization rate to three times faster than that of the neat polymer. This was attributed to enhanced dispersion and reduced aggregation of the nanofillers in the polymer matrix. Polarized optical microscopy shows little difference in spherulite growth rate among the composites, supporting the theory that heterogeneous nucleation and higher surface area are responsible for the faster overall growth in crystallinity.

In DMTA studies, both MWCNT and CNS raise the modulus of PLA and increase the HDT by $\sim$ 10°C; however, no change in glass transition is observed in DSC analysis. This finding indicates suboptimal segmental interaction between the polymer and the nanofillers. That is, the PLA is not strongly bound to any of the carbon nanostructures.

CNS and MWCNT may have advantages other than enhancement of thermal and mechanical properties as fillers for renewable, biocompatible PLA polymers. Grafted functionalities on the nanoparticle surfaces not only yield increased control over the dispersion in polymer matrices, but also could include active molecules for medical, sensing, optical, and electrical properties. Optimum functionalities and filler loading levels naturally depend on the intended application and target properties.

References

1. Jeong, W.; Kessler, M. R. Chem Mater 2008, 20, 7060.
2. Wang, C.; Guo, Z.-X.; Fu, S.; Wu, W.; Zhu, D. Progr Polym Sci 2004, 29, 1079.
3. Biercuk, M. J.; Llaguno, M. C.; Radosavljevic, M.; Hyun, J. K.; Johnson, A. T. Appl Phys Lett 2002, 80, 2767.
4. Breuer, O.; Sundararaj, U. Polym Compos 2004, 25, 630.
5. Baughman, R. H.; Zakhidov, A. A.; de Heer, W. A. Science 2002, 297, 787.
6. Prato, M.; Kostarelos, K.; Bianco, A. Acc Chem Res 2007, 41, 60.
7. Ago, H.; Petritsch, K.; Shaffer, M. S. P.; Windle, A. H.; Friend, R. H. Adv Mater 1999, 11, 1281.
8. Chin, K. C.; Gohel, A.; Elim, H. I.; Chen, W.; Ji, W.; Chong, G. L.; Sow, C. H.; Wee, A. T. S. J Mater Res 2006, 21, 2758.
9. Dai, L. Carbon Nanotechnology: Recent Developments in Chemistry, Physics, Materials Science and Device Applications; Elsevier: Amsterdam, Netherlands, 2006.
10. Ajayan, P. M.; Schadler, L. S.; Braun, P. V. Nanocomposite Science and Technology; Wiley-VCH: Morlenbach, 2003.
11. Chen, J.; Rao, A.; Lyuksyutov, S.; Itkis, M. E.; Hamon, M. A.; Hu, H.; Cohn, R. W.; Eklund, P. C.; Colbert, D. T.; Smalley, R. E.; Haddon, R. C. J Phys Chem B 2001, 105, 2525.
12. Dalton, A. B.; Collins, S.; Munoz, E.; Razal, J. M.; Ebron, V. H.; Ferraris, J. P.; Coleman, J. N.; Kim, B. G.; Baughman, R. H. Nature 2003, 423, 703.
13. Vigolo, B.; Penicaud, A.; Coulon, C.; Sauder, C.; Pailler, R.; Journet, C.; Bernier, P.; Poulin, P. Science 2000, 290, 1331.
14. Strano, M. Nat Mater 2006, 5, 433.
15. Moniruzzaman, M.; Winey, K. I. Macromolecules 2006, 39, 5194.
16. Xie, X.-L.; Mai, Y.-W.; Zhou, X.-P. Mater Sci Eng R Rep 2005, 49, 89.
17. Lopez-Manchado, M. A.; Valentini, L.; Biagiotti, J.; Kenny, J. M. Carbon 2005, 43, 1499.
18. Jin, Z.; Pramoda, K. P.; Xu, G.; Goh, S. H. Chem Phys Lett 2001, 337, 43.
19. Velasco-Santos, C.; Martinez-Hernandez, A. L.; Fisher, F.; Ruoff, R.; Castano, V. M. J Phys Appl Phys 2003, 36, 1423.
20. Gojny, F. H.; Schulte, K. Compos Sci Technol 2004, 64, 2303.
21. Dorgan, J. R.; Braun, B.; Wegner, J. R.; Knauss, D. M. In ACS Symposium: Degradable Polymers and Materials—Principles and Practice; Khemani, K. C.; Scholz, C., Eds.; American Chemical Society: Washington, D.C., 2006, 102–125.
22. Auras, R.; Harte, B.; Selke, S. Macromol Biosci 2004, 4, 835.
23. Herring, A. M.; McKinnon, J. T.; McCloskey, B. D.; Filley, J.; Gneshin, K. W.; Pavelka, R. A.; Kleebe, H.-J.; Aldrich, D. J. J Am Chem Soc 2003, 125, 9916.
24. Arkema To Build Carbon Nanotube Pilot Plant In France, Reuters; Colombes, France, 17 Sept 2009.
25. Sobkowicz, M. J.; Dorgan, J. R.; Gneshin, K. W.; Herring, A. M.; McKinnon, J. T. Aust J Chem 2009, 62, 865.
26. Song, W.; Zheng, Z.; Tang, W.; Wang, X. Polymer 2007, 48, 3658.
27. Mandelkern, L. Physical Properties of Polymers; Cambridge University Press: Cambridge, UK, 2003.
28. Tsuji, H.; Miyauchi, S. Biomacromolecules 2001, 2, 597.

29. Tsuji, H. Biomaterials 2003, 24, 537.
30. Hartmann, M. H. In Biopolymers from Renewable Resources; Kaplan, D. L., Ed.; Springer, 1998, 367–412.
31. Sobkowicz, M. J.; Dorgan, J. R.; Gneshin, K. W.; Herring, A. M.; McKinnon, J. T. J Polym Environ 2008, 16, 131.
32. Su, Z.; Guo, W.; Liu, Y.; Li, Q.; Wu, C. Polym Bull 2009, 62, 629.
33. Hu, X.; An, H.; Li, Z.-M.; Geng, Y.; Li, L.; Yang, C. Macromolecules 2009, 42, 3215.
34. Grady, B. P.; Pompeo, F.; Shambaugh, R. L.; Resasco, D. E. J Phys Chem B 2002, 106, 5852.
35. Mucha, M.; Marszalek, J.; Fidrych, A. Polymer 1999, 41, 4137.
36. Bhattacharyya, A. R.; Sreekumar, T. V.; Liu, T.; Kumar, S.; Ericson, L. M.; Hauge, R. H.; Smalley, R. E. Polymer 2003, 44, 2372.
37. Assouline, E.; Lustiger, A.; Barber, A. H.; Cooper, C. A.; Klein, E.; Wachtel, E.; Wagner, H. D. J Polym Sci Part B: Polym Phys 2002, 41, 520.
38. Anand, K. A.; Agarwal, U. S.; Joseph, R. Polymer 2006, 47, 3976.
39. Kim, J. Y.; Park, H. S.; Kim, S. H. Polymer 2006, 47, 1379.
40. Day, M.; Nawaby, A. V.; Liao, X. J Therm Anal Calorim 2006, 86, 623.
41. Kolstad, J. J. J Appl Polym Sci 1996, 62, 1079.
42. Schmidt, S. C.; Hillmyer, M. A. J Polym Sci Part C: Polym Phys 2000, 39, 300.
43. Urayama, H.; Kanamori, T.; Fukushima, K.; Kimura, Y. Polymer 2003, 44, 5635.
44. MacDonald, R. T.; McCarthy, S. P.; Gross, R. A. Macromolecules 1996, 29, 7356.
45. Sobkowicz, M. J.; Dorgan, J. R.; Gneshin, K. W.; Herring, A. M.; McKinnon, J. T. Carbon 2008, 47, 622.
46. Fischer, E. W.; Sterzel, H. J.; Wegner, G. Kolloid-Z.u.Z Polymere 1973, 251, 980.
47. Takemori, M. T. Polym Eng Sci 1979, 19, 1104.